Electronic Supplementary Material (ESI) for Energy & Environmental Science.

# Supporting Information

# Inhibiting Metal-Inward Diffusion-Induced Degradation through Strong Chemical Coordination toward Stable and Efficient Inverted Perovskite Solar Cells

Jiabao Yang,[a] Qi Cao,[a] Tong Wang,[a] Bowen Yang,[b,c] Xingyu Pu,[a] Yixin Zhang,[a] Hui Chen,[a] Ilhom Tojiboyev,[d] Yuke Li,[e] Lioz Etgar,[f] Xuanhua Li,[a]* Anders Hagfeldt[b,c]

[a] State key Laboratory of Solidification Processing, Center for Nano Energy Materials, School of Materials Science and Engineering, Northwestern Polytechnical University, Xi´an 710072, People's Republic of China

*Email address: lixh32@nwpu.edu.cn

[b] Department of Chemistry-Ångström Laboratory, Uppsala University, SE-75120 Uppsala, Sweden

[c] Laboratory of Photomolecular Science, Institute of Chemical Sciences and Engineering, School of Basic Sciences, Ecole Polytechnique Fédérale de Lausanne, CH-1015 Lausanne, Switzerland

[d] Institute Ion - Plasma and Laser Technologies, Uzbekistan Academy of Sciences, 100125, Durmon yuli 33 Tashkent, Uzbekistan

[e] Department of Chemistry and Centre for Scientific Modeling and Computation, Chinese University of Hong Kong, Shatin, Hong Kong, China

[f] Institute of Chemistry, Casali Center for Applied Chemistry, The Hebrew University of Jerusalem, Jerusalem 91904, Israel

## Experimental Procedures

### Materials

N, N-dimethylformamide (DMF, 99.8%), Chlorobenzene (CB, 99.8%), anhydrous dimethyl sulfoxide (DMSO, 99.8%) and isopropanol (IPA, 99.9%) were purchased via Sigma-Aldrich. TTTS (98%) was purchased from Macklin (Shanghai). $NiO_x$ powder was obtained according to reported preparation method.[1] And other materials were obtained via Xi'an Polymer Light Technology Corp.

### Device fabrication

The ITO glass was successively washed for 15 min by deionized water, acetone, ethanol and dried with nitrogen. After spin-coating $NiO_x$ film (20 nm), the perovskite precursor solution (triple cation halide perovskite was blended by 0.21 M methylammonium bromide (MABr), 1.19 M formamidine iodide (FAI), 0.21 M lead bromide ($PbBr_2$), 0.7 M cesium iodide (CsI) and 1.30 M lead iodide ($PbI_2$) in DMF/DMSO (4/1 V/V)) was spin-coated at 1000 rpm, 10 s and 6000 rpm, 30 s in a $N_2$-filled glove box, then an anti-solvent CB (chlorobenzene) was dripped after 30 s. The perovskite film was obtained by annealing (100 °C, 20 min). Then the PCBM:$C_{60}$ solution was prepared via blending PCBM /$C_{60}$ (20 mg /5 mg) in 1 mL CB and spin-coated for PCBM:C60 film (3000 rpm, 40 s). The BCP solutions (0.5 mg $mL^{-1}$ in isopropanol) with different concentrations of TTTS were spin-coated at 5800 rpm for 60 s to obtain BCP layer (10 nm). At last, Au (100 nm) was thermally deposited. The effective area of the device was 0.1 $cm^2$.

As for the devices with Cu or Ag electrode, the thickness of Cu or Ag was set to 90 or 100 nm, respectively. The rest of the functional layers were prepared as described above.

As for the conventional devices, $SnO_2$ was obtained according to reported preparation method.[2] The $SnO_2$ solution was spin-coated at 6000 rpm, 35 s and heated at 180 °C in the air (1 h) to obtain a $SnO_2$ film. The spiro-MeOTAD (2,2',7,7'-tetrakis(N,N-di-p-methoxyphenylamine)-9,9'-spirobifluorene) precursor solution was obtained via dissolving 90 mg of spiro-MeOTAD powder, 22 μL of 4-t-butylpyridine and 36 μL of lithium bis (trifluoromethanesulfonyl) imide solution pre-configured in acetonitrile (520 mg/mL) in chlorobenzene (1 mL). The spin-coating parameter was 4000 rpm for 30 s.

## Characterizations

The *J-V* curves of devices (0.1 cm$^2$ effective area, scan rate was 0.1 V s$^{-1}$) were conducted by a keithley 2420 sourcemeter, and a solar simulator (100 mW cm$^{-2}$, Newport 94023A Oriel Sol3A, Class AAA) with AM 1.5G illumination (regulated via a standard silicon cell (Hamamatsu S1133)). The EQE was performed from 300 to 800 nm via monochromatic incident light (Newport, 1600 W). The characterization of film morphology and conductivity was conducted from SEM (FEI 4S50) and AFM (Bruker, Dimension Icon). The perovskite films of C-AFM test were obtained by stripping the Au electrode with Kapton tape and spin-coating CB to remove ETL. A cross-sectional TEM images and EDX mapping were obtain from TEM (FEI, Talos F200X) and samples were pre-processed via FIB (Helios G4 CX) milling. TPV and TPC characterizations were conducted via a digital oscilloscope and picosecond pulse laser (Agilent Technologies, DSO71048). The XPS and UPS spectra were conducted by Kratos instrument (Axis Supra). EIS spectra was obtained by an electrochemical workstation (Chenhua 760, China). The semiconductor band gap was performed via Shimadzu instruments (UV-3510). The operational stability was record by a MPP trace system (YH-VMPP-16).

## Stability test

The ambient stability was conducted at 25 °C and 50 ± 5% RH without encapsulation. The thermal stability of devices was performed in a N$_2$-filled glove box at 85 °C without encapsulation. The average PCE and standard error are calculated from ten devices. As for *J-V* characterization, the PSCs were cooled to room temperature and measured via a Newport solar simulator at different time intervals. The operational stability of encapsulated devices was conducted via a light-emitting diode lamp (no UV filter) to provide continuous one-sun illumination at 45 °C to track the MPP via a MPP trace system (YH-VMPP-16). As for the encapsulation of devices in operational stability, it can be achieved via UV adhesive (LT-U001, Lumtec) and a glass on top.

## Results and Discussion

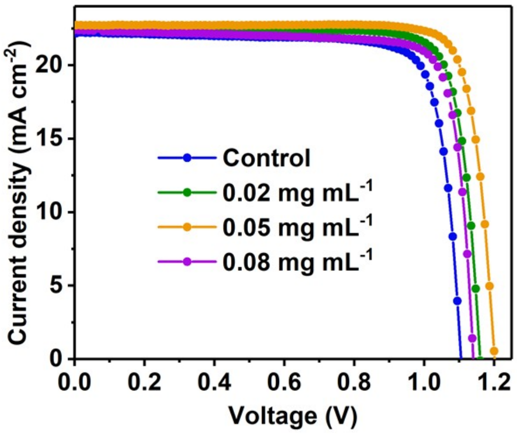

**Figure S1.** The *J-V* characterization of devices with different concentration of TTTS in BCP layer.

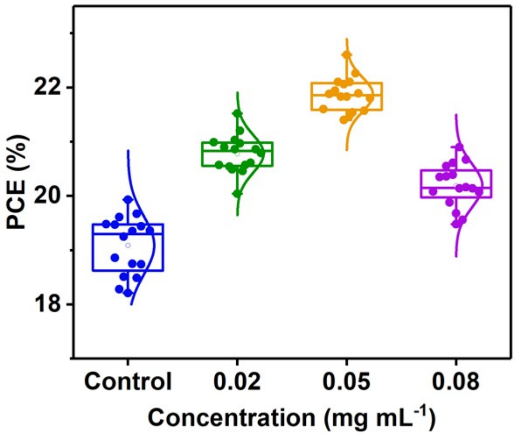

**Figure S2.** Statistical PCE of the devices with different concentration of TTTS in BCP layer.

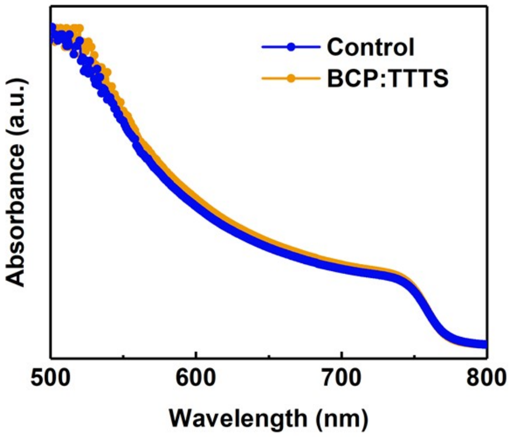

**Figure S3.** The UV-Vis absorption spectra for devices with structure of CsFAMA /PCBM:$C_{60}$ /BCP.

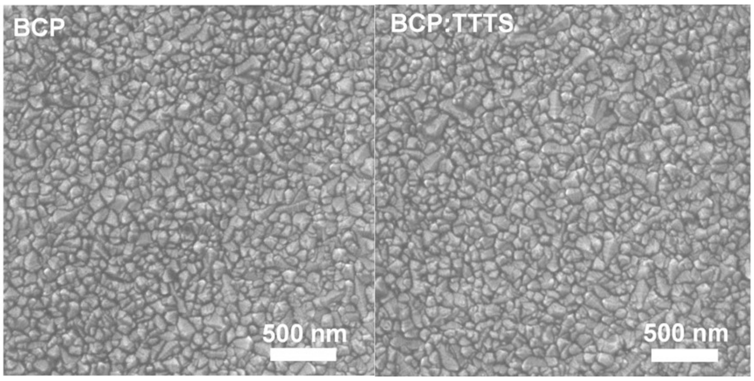

**Figure S4.** The SEM images of BCP and BCP:TTTS films.

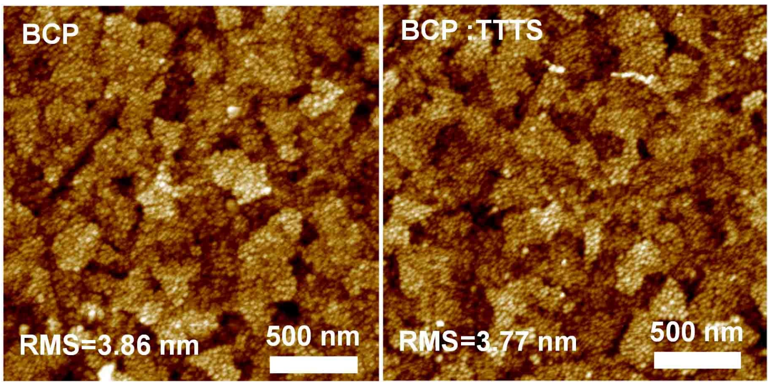

**Figure S5.** The AFM images of BCP and BCP:TTTS films. The images indicate that the RMS surface roughness is basically the same for BCP:TTTS film (3.77 nm) compared with BCP film (3.86 nm).

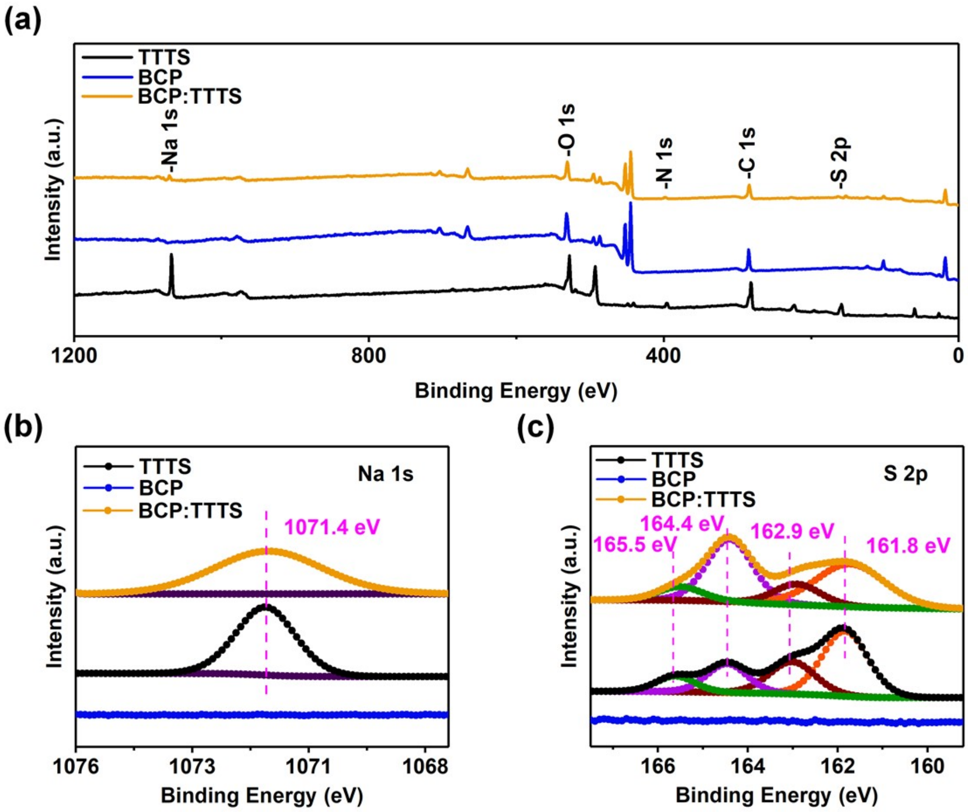

**Figure S6.** The XPS analysis of TTTS, BCP, and BCP:TTTS films. (a) The full XPS spectra. (b) Na 1s spectra. (c) S 2p spectra. The peaks do not shift, which indicates that there is no interaction between BCP and TTTS.

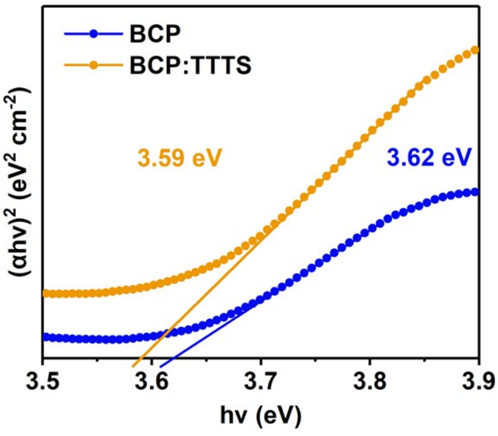

**Figure S7.** Tauc plots of $(\alpha h\nu)^2$ versus hν.

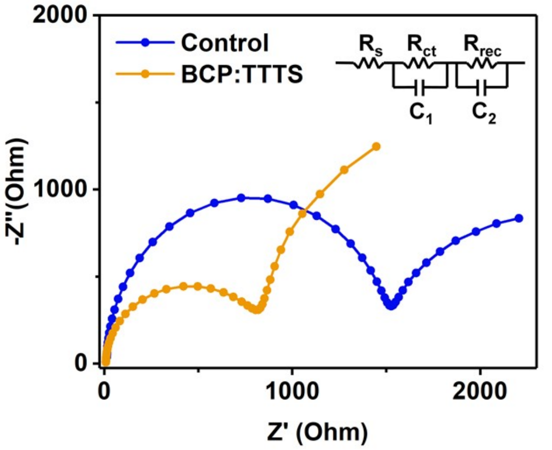

**Figure S8.** The Nyquist plots recorded in the dark and the inset is the equivalent circuit. The high-frequency and low-frequency of the Nyquist plots correspond to the charge transport resistance (Rct) and the recombination resistance (Rrec), respectively. The smaller Rct (1002 Ω) and larger Rrec (4599 Ω) of BCP:TTTS device than Control (1558 and 2995 Ω, respectively) indicate more efficient electron transport and less carrier recombination.

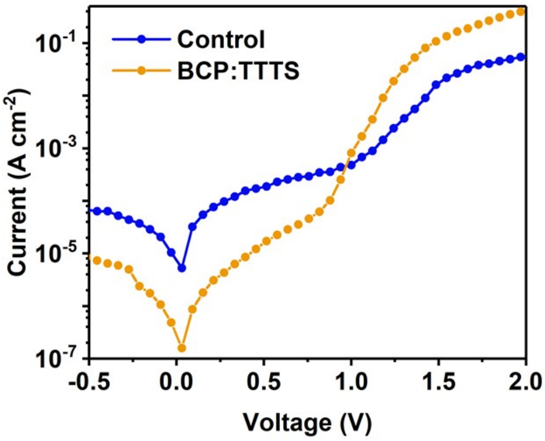

**Figure S9.** The dark *J-V* characterization of devices without or with TTTS in BCP layer. The lower leakage current reveals that electrons are more effectively extracted instead of recombination in BCP:TTTS device.

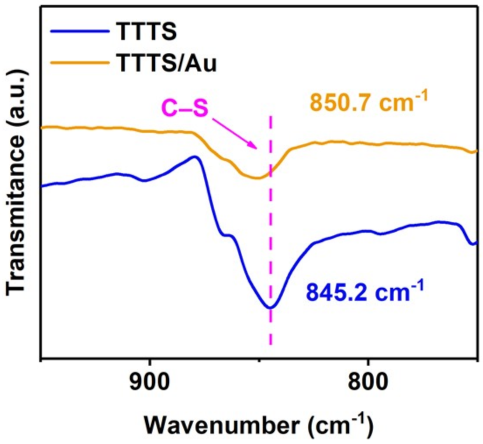

**Figure S10.** The FTIR of TTTS and TTTS /Au films. The weak C-S bond peak is due to 20 nm Au film above the TTTS film, reducing light intensity from FTIR instrument.

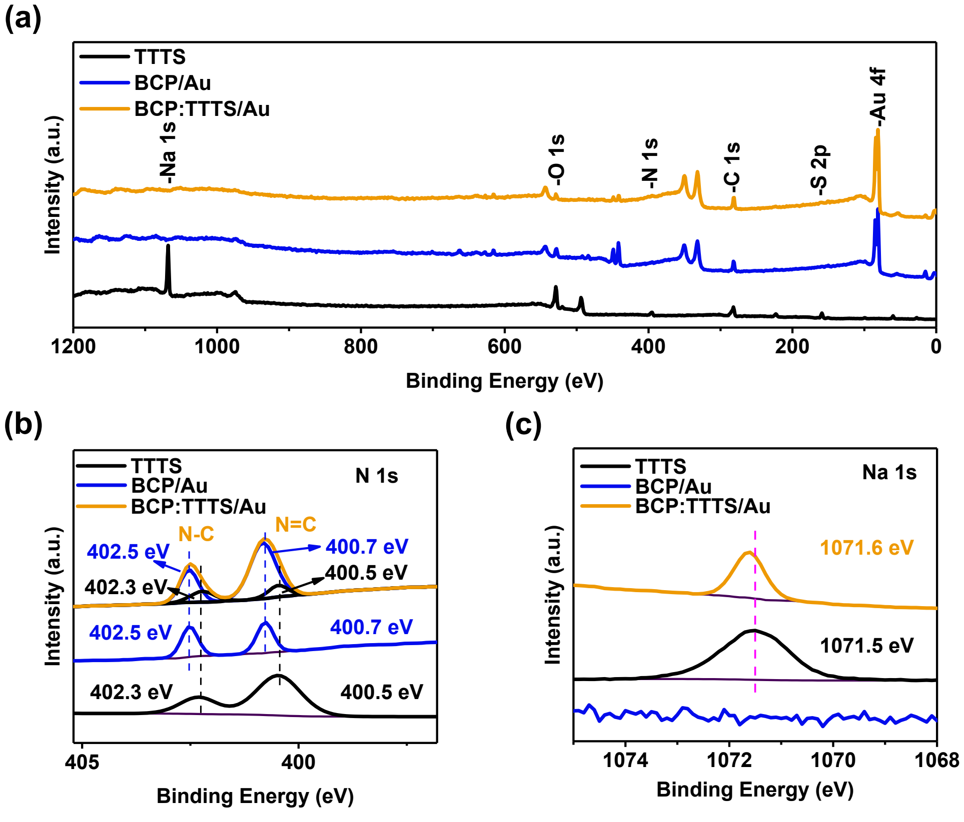

**Figure S11.** The XPS analysis of TTTS, BCP /Au, and BCP:TTTS /Au film. (a) The full XPS spectra. (b) N 1s spectra. (c) Na 1s spectra. As shown in **Figure S11b**, TTTS has two main N 1s peaks located at 402.3 and 4005 eV corresponding to N-C and N=C, respectively. In addition, BCP film has two peaks located at 402.5 and 4007 eV for N-C and N=C, respectively. The deconvolution of N 1s XPS spectra for BCP:TTTS /Au film indicates two different chemical environments of N atoms corresponding to TTTS and BCP, respectively after blending TTTS and BCP. The peaks of N 1s are not shift before and after adding TTTS additive, which means that there is no interaction between N in TTTS and metal electrode. The main reason is the conjugation system of triazine ring caused by N-C and N=C, which reduces the electron cloud density around N atoms.

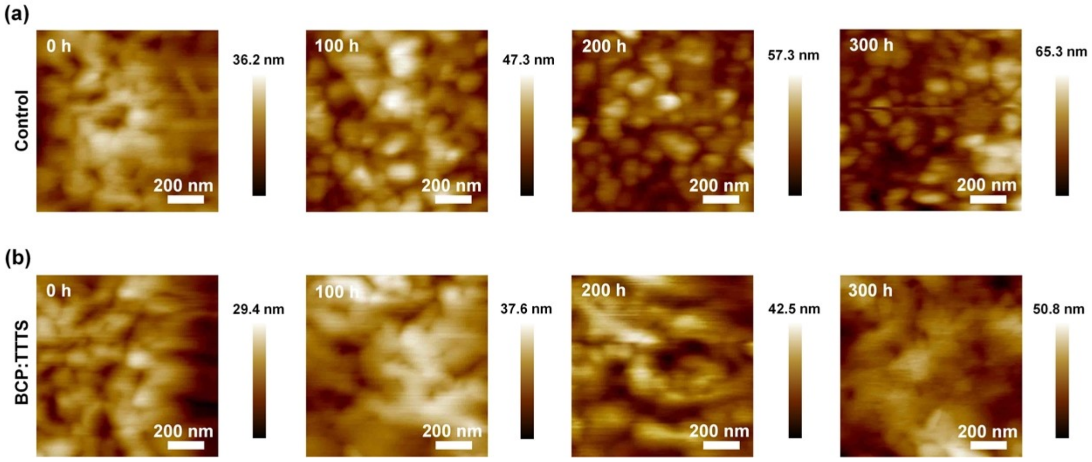

**Figure S12.** The corresponding C-AFM topographic images of perovskite films obtained from the PSCs (a) without or (b) with TTTS after different heating time (0, 100, 200 or 300 h).

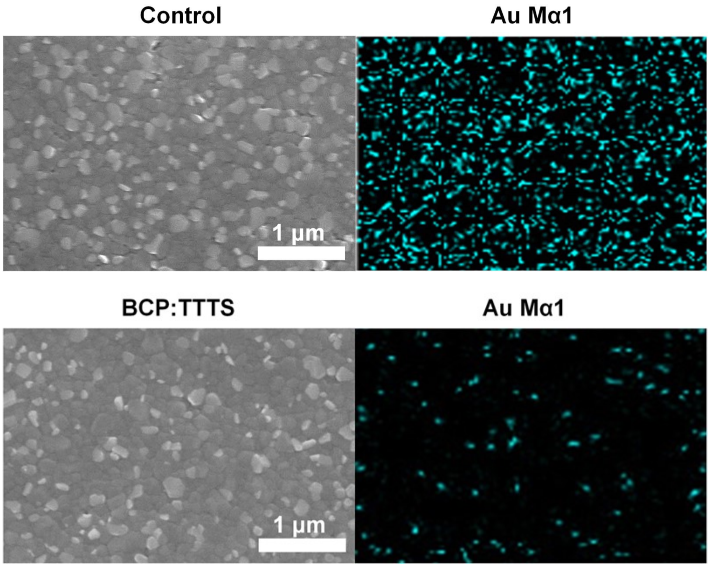

**Figure S13.** The SEM images and the corresponding EDX mapping of the aging perovskite films after 300 h continue heating from C-AFM test.

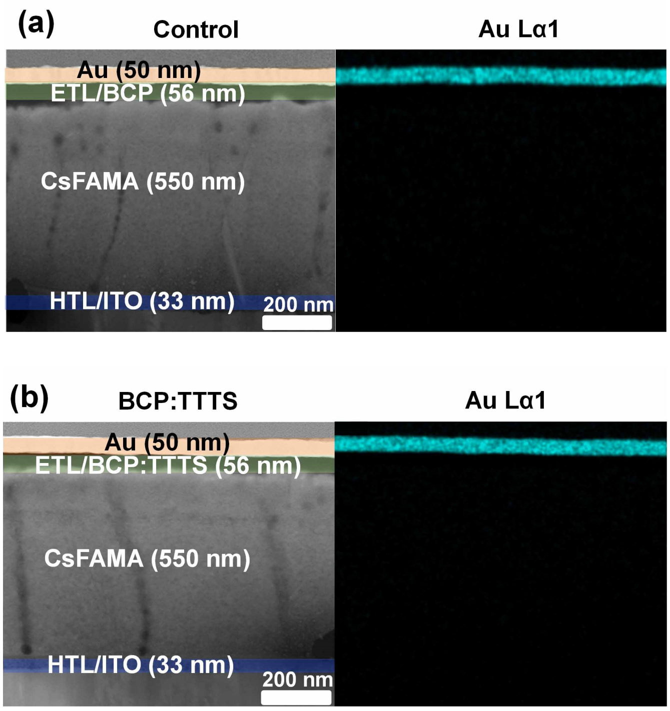

**Figure S14.** The cross-sectional STEM and EDX analysis of the pristine devices (a) without or (b) with TTTS.

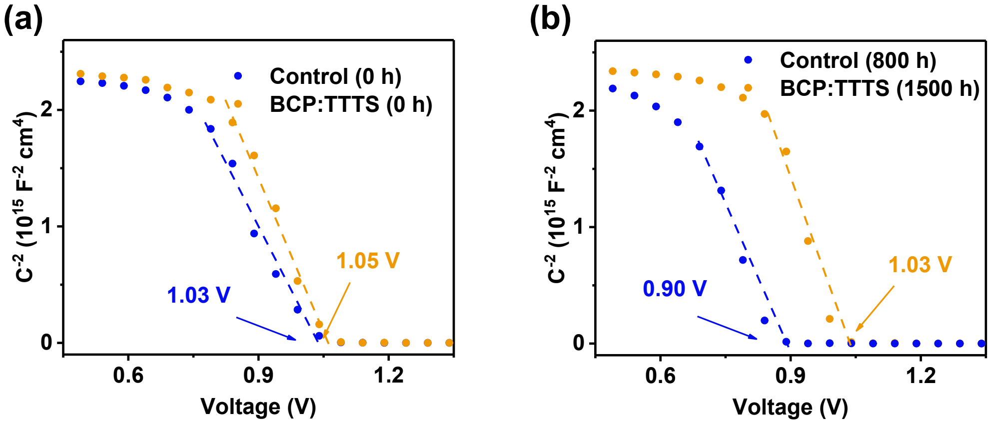

**Figure S15.** The Mott-Schottky plots of the PSCs (a) before and (b) after thermal stability test.

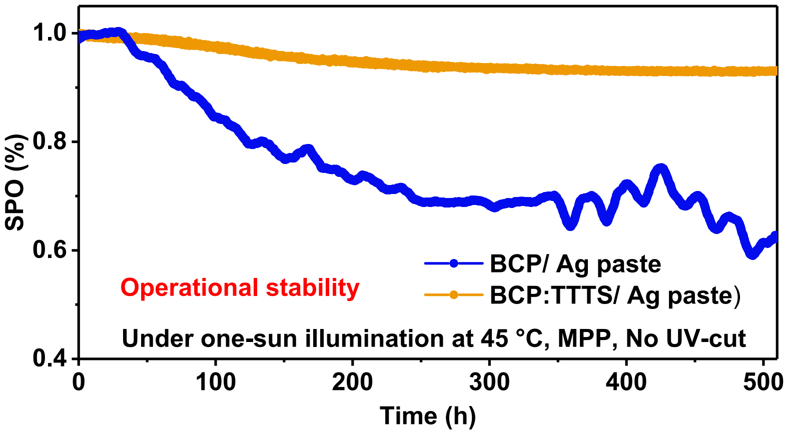

**Figure S16.** The operational stability of devices with Ag paste. The operational stability test of encapsulated devices is conducted under one-sun illumination without UV (ultraviolet) filter at 45 °C to track the MPP. The SPO traces are the degradation of a single champion device for Control and BCP:TTTS devices.

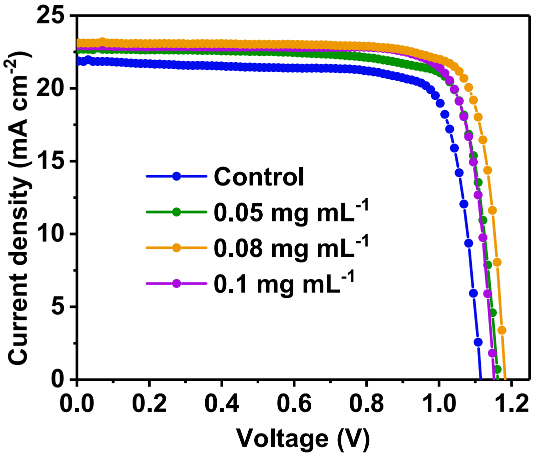

**Figure S17.** The *J-V* curves of conventional devices with different concentration of TTTS in Spiro-OMeTAD layer. The structure of PSCs is ITO /$SnO_2$ /CsFAMA perovskite /Spiro-OMeTAD without or with TTTS /Au.

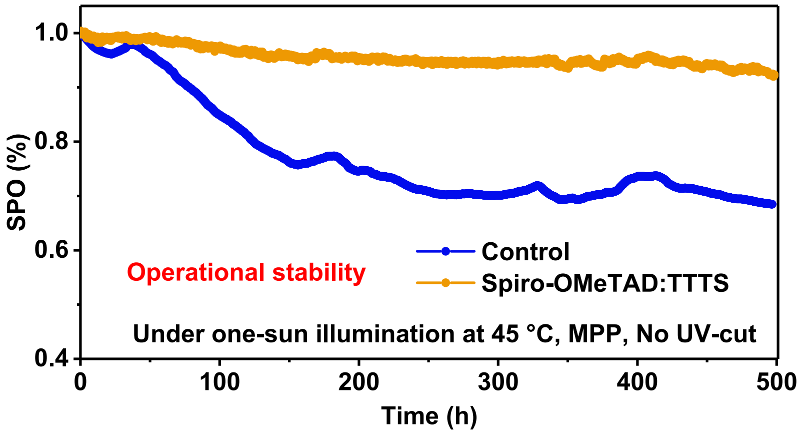

**Figure S18.** The operational stability of conventional champion devices. The operational stability test of encapsulated devices is conducted under one-sun illumination without UV (ultraviolet) filter at 45 °C to track the MPP. The SPO traces are the degradation of a single champion device for Control and Spiro-OMeTAD:TTTS devices. Spiro-OMeTAD:TTTS represents the Spiro-OMeTAD layer with TTTS.

**Table S1.** Photovoltaic parameters of the devices with different concentration of TTTS additive in BCP layer (Data in brackets are the average values of each parameter for 15 devices). The scan rate is 0.1 V s$^{-1}$.

| Device<br>[mg mL$^{-1}$] | $V_{OC}$<br>[V] | $J_{SC}$<br>[mA cm$^{-2}$] | FF<br>[%] | PCE<br>[%] |
|---|---|---|---|---|
| Control | 1.11 | 22.24 | 80.74 | 19.93 |
| | (1.10 ± 0.02) | (21.73 ± 0.24) | (79.95 ± 0.42) | (19.09 ± 0.54) |
| 0.02 | 1.16 | 22.52 | 82.07 | 21.42 |
| | (1.16 ± 0.02) | (22.08 ± 0.18) | (81.51 ± 0.38) | (20.68 ± 0.35) |
| 0.05 | 1.20 | 22.73 | 82.84 | 22.59 |
| | (1.20 ± 0.01) | (22.35 ± 0.17) | (82.36 ± 0.34) | (21.87 ± 0.31) |
| 0.08 | 1.14 | 22.39 | 81.70 | 20.86 |
| | (1.14 ± 0.01) | (22.03 ± 0.20) | (81.24 ± 0.41) | (20.15 ± 0.40) |

**Table S2.** Photovoltaic parameters of the large area devices (1 cm$^2$) (Data in brackets are the average values of each parameter for 15 devices). The scan rate is 0.1 V s$^{-1}$.

| Device | | $V_{OC}$<br>[V] | $J_{SC}$<br>[mA cm$^{-2}$] | FF<br>[%] | PCE<br>[%] |
|---|---|---|---|---|---|
| Control | F [a] | 1.07 | 19.46 | 75.45 | 15.72 |
| | | (1.05 ± 0.03) | (19.08 ± 0.28) | (74.84 ± 0.52) | (15.56 ± 0.63) |
| | R [b] | 1.08 | 20.32 | 76.90 | 16.85 |
| | | (1.06 ± 0.03) | (19.86 ± 0.26) | (76.38 ± 0.49) | (15.92 ± 0.60) |
| BCP:TTTS | F [a] | 1.16 | 21.25 | 79.38 | 19.29 |
| | | (1.16 ± 0.02) | (20.91 ± 0.26) | (77.68 ± 0.44) | (18.68 ± 0.39) |
| | R [b] | 1.17 | 21.74 | 79.48 | 20.21 |
| | | (1.17 ± 0.02) | (21.45 ± 0.22) | (78.96 ± 0.40) | (19.58 ± 0.36) |

[a] The forward scan direction.

[b] The reverse scan direction.

**Table S3.** The checklist for reporting data from operational stability test.

| Key aspects | Characteristics | Details |
|---|---|---|
| Initial solar cell characterization | Current–voltage (J–V) curves | The J-V reverse curves (scan rate was 0.1 V $s^{-1}$) are conducted by a white light-emitting diode lamp (100 mW $cm^{-2}$). |
| Encapsulation | Front- and back-side encapsulation layer(s) and edge sealant | A cover glass on back side and UV adhesive (LT-U001, Lumtec) at edge. |
| Ageing conditions | Light | A white light-emitting diode lamp (100 mW $cm^{-2}$). |
|  | Temperature | 45 °C |
|  | Atmosphere | Air |
| Measurements during ageing | MPP tracking | It is tested by thin-film photovoltaic maximum power point tracking test system (YH-VMPP-16) at regular intervals |
| Number of samples |  | The champion device |

**Table S4.** The checklist for reporting data from ambient stability test.

| Key aspects | Characteristics | Details |
|---|---|---|
| Initial solar cell characterization | Current–voltage (J–V) curves | The J-V curves (scan rate was 0.1 V $s^{-1}$) were conducted by a keithley 2420 sourcemeter, and a solar simulator (100 mW $cm^{-2}$, Newport 94023A Oriel Sol3A, Class AAA) with AM 1.5G illumination. |
| Ageing conditions | Temperature | 25 °C, 50 ± 5% relative humidity |
|  | Atmosphere | Air |
| Measurements during ageing | Periodically recorded J–V curves | For J-V curves, the devices were tested at different time intervals via a solar simulator (100 mW $cm^{-2}$, Newport 94023A Oriel Sol3A, Class AAA) with AM 1.5G illumination. |
| Number of samples |  | 10 |

**Table S5.** The checklist for reporting data from thermal stability test.

| **Key aspects** | **Characteristics** | **Details** |
|---|---|---|
| Initial solar cell characterization | Current–voltage (J–V) curves | The J-V curves (scan rate was 0.1 V $s^{-1}$) were conducted by a keithley 2420 sourcemeter, and a solar simulator (100 mW $cm^{-2}$, Newport 94023A Oriel Sol3A, Class AAA) with AM 1.5G illumination. |
| Ageing conditions | Temperature<br>Atmosphere | 85 °C<br>$N_2$-filled glove box |
| Measurements during ageing | Periodically recorded J–V curves | For J-V curves, the devices were taken out of the glove box, then cooled and tested at different time intervals via a solar simulator (100 mW $cm^{-2}$, Newport 94023A Oriel Sol3A, Class AAA) with AM 1.5G illumination. |
| Number of samples | | 10 |

**Table S6.** Photovoltaic parameters of the devices with Cu electrode (Data in brackets are the average values of each parameter for 15 devices). The scan rate is 0.1 V $s^{-1}$.

| Device | | $V_{OC}$ [V] | $J_{SC}$ [mA $cm^{-2}$] | FF [%] | PCE [%] |
|---|---|---|---|---|---|
| BCP/Cu | F [a] | 1.09<br>(1.08 ± 0.02) | 20.98<br>(20.52 ± 0.26) | 79.69<br>(78.85 ± 0.47) | 18.22<br>(17.33 ± 0.58) |
| | R [b] | 1.10<br>(1.09 ± 0.02) | 21.62<br>(21.16 ± 0.24) | 80.45<br>(79.63 ± 0.44) | 19.11<br>(18.32 ± 0.55) |
| BCP:TTTS/Cu | F [a] | 1.13<br>(1.13 ± 0.01) | 22.24<br>(21.76 ± 0.22) | 81.16<br>(80.57 ± 0.37) | 20.42<br>(19.78 ± 0.36) |
| | R [b] | 1.15<br>(1.15 ± 0.01) | 22.49<br>(22.08 ± 0.19) | 82.39<br>(81.71 ± 0.35) | 21.31<br>(20.86 ± 0.33) |

[a] The forward scan direction.

[b] The reverse scan direction.

**Table S7.** Photovoltaic parameters of the devices with Ag electrode (Data in brackets are the average values of each parameter for 15 devices). The scan rate is 0.1 V $s^{-1}$.

| Device | | $V_{OC}$ [V] | $J_{SC}$ [mA $cm^{-2}$] | FF [%] | PCE [%] |
|---|---|---|---|---|---|
| BCP/Ag | F [a] | 1.10<br>(1.09 ± 0.02) | 21.38<br>(20.95 ± 0.29) | 79.53<br>(78.72 ± 0.45) | 18.77<br>(17.81 ± 0.54) |
| | R [b] | 1.11<br>(1.10 ± 0.02) | 22.11<br>(21.43 ± 0.26) | 80.06<br>(79.28 ± 0.42) | 19.66<br>(18.73 ± 0.51) |
| BCP:TTTS/ Ag | F [a] | 1.15<br>(1.15 ± 0.02) | 22.11<br>(21.57 ± 0.24) | 81.10<br>(80.49 ± 0.34) | 20.65<br>(19.82 ± 0.34) |
| | R [b] | 1.16<br>(1.16 ± 0.01) | 22.62<br>(22.04 ± 0.21) | 82.17<br>(81.63 ± 0.32) | 21.53<br>(20.91 ± 0.32) |

[a] The forward scan direction.

[b] The reverse scan direction.

## References

1. W. Chen, Y. Zhou, L. Wang, Y. Wu, B. Tu, B. Yu, F. Liu, H. W. Tam, G. Wang, A. B. Djurisic, L. Huang, Z. He, *Adv. Mater.* 2018, **30**, 1800515.
2. Q. Cao, Z. Li, J. Han, S. Wang, J. Zhu, H. Tang, X. Li, X. Li, *Sol. RRL* 2019, **3**, 1900333.